eNeuro

Research Article: New Research | Integrative Systems

Social Experience Interacts with Serotonin to Affect Functional Connectivity in the Social Behavior Network following Playback of Social Vocalizations in Mice

https://doi.org/10.1523/ENEURO.0247-20.2021

Cite as: eNeuro 2021; 10.1523/ENEURO.0247-20.2021

Received: 9 June 2020
Revised: 2 February 2021
Accepted: 15 February 2021

Manuscript Title: Social experience interacts with serotonin to affect functional connectivity in the social behavior network following playback of social vocalizations in mice

Abbreviated Title: Experience and serotonin affect functional connectivity

Authors: Christopher L. Petersen[1,2], Sarah E. D. Davis[1], Bhumi Patel[1], and Laura M. Hurley[1,2,3]

[1]Indiana University, Bloomington – Department of Biology
[2]Indiana University, Bloomington – Center for the Integrative Study of Animal Behavior
[3]Indiana University, Bloomington – Department of Neuroscience

Author Contributions: CLP and LMH designed research, CLP, SEDD, and BP performed research, CLP analyzed data and wrote the paper, LMH supervised project.

Corresponding author (Current address):
Christopher L. Petersen, Ph.D.
University of Minnesota
Department of Neuroscience and Medical Discovery Team on Addiction
McGuire Translational Research Facility
2001 6th Street, SE
Minneapolis, MN 55455
chlpete@umn.edu

Number of figures: 6 (plus 2 extended data tables)

Number of tables: 2

Number of multimedia: 0

Number of words for abstract: 233

Number of words in significance statement: 117

Number of words for introduction: 746

Number of words for discussion: 2431

Acknowledgements: The authors wish to thank Jim Powers Ph.D. in the Indiana University Light Microscopy Imaging Center (LMIC) for technical support, Richard Betzel Ph.D. for network advice, Kelly Ronald, Ph.D. and Anna Ingebretson Ph.D. for

comments on the original manuscript, and members of the Hurley Lab for helpful discussions.

Dedication: This publication is inspired by and dedicated to the memory of James L. Goodson, Ph.D. (1965 – 2014).

Conflict of Interest: Authors report no conflicts of interest

Funding sources: This work was supported by the National Institute of Health Common Themes in Reproductive Diversity Training Grant (5T32HD049336-12), the Indiana University College of Arts and Sciences, and the Center for the Integrative Study in Animal Behavior (CLP), and NSF grant IOS 1456298 (LMH).

Abstract

Past social experience affects the circuitry responsible for producing and interpreting current behaviors. The social behavior network (SBN) is a candidate neural ensemble to investigate the consequences of early-life social isolation. The SBN interprets and produces social behaviors, such as vocalizations, through coordinated patterns of activity (functional connectivity) between its multiple nuclei. However, the SBN is relatively unexplored with respect to murine vocal processing. The serotonergic system is sensitive to past experience and innervates many nodes of the SBN; therefore, we tested whether serotonin signaling interacts with social experience to affect patterns of immediate early gene (cFos) induction in the male SBN following playback of social vocalizations. Male mice were separated into either social housing of 3 mice per cage or into isolated housing at 18 – 24 days postnatal. After 28 – 30 days in housing treatment, mice were parsed into 1 of 3 drug treatment groups: control, fenfluramine (increases available serotonin) or pCPA (depletes available serotonin) and exposed to a 60-minute playback of female broadband vocalizations. Fenfluramine generally increased the number of cFos immunoreactive neurons within the SBN, but effects were more pronounced in socially isolated mice. Despite a generalized increase in cFos immunoreactivity, isolated mice had reduced functional connectivity, clustering, and modularity compared to socially reared mice. These results are analogous to observations of functional dysconnectivity in persons with psychopathologies and suggests that early-life social isolation modulates serotonergic regulation of social networks.

Significance Statement

Social isolation and serotonergic signaling each modulate neural functions independently of each other. It is unknown whether these factors interact to affect activity at the level of individual nuclei, and/or functional networks. Using a vocal playback paradigm, we find that acutely increasing or systemically depleting available serotonin increased cFos immunoreactive neurons in the social behavior network (SBN) mice raised in social isolation compared to their socially reared counterparts. We show for the first time that mice raised in social isolation have reduced functional connectivity in the SBN relative to socially reared mice. Importantly, network perturbations were not resolved by drug treatment in isolated mice suggesting that social experience is necessary to facilitate functional relationships in the SBN.

Introduction

The importance of social rearing has been evident since the 1960's and the now-controversial "Harlow monkey experiments," which demonstrated that early-life social isolation deprives macaques of the experiences necessary to develop into functional adults (Harlow et al., 1965). The ability to amicably behave and communicate with conspecifics is important to social cohesion, which in turn affects individual fitness and psychological wellness (Heim and Nemeroff, 2001; Bailey and Moore, 2018). Neural systems have evolved to support social cohesion (Goodson, 2013; Matthews and Tye, 2019) such that social interactions may carry positive valence (Goodson and Wang, 2006),

and be reinforced by the brain's reward circuitry (Dolen et al., 2013). Early-life social immersion or deprivation may shape the circuits responsible for the appropriate expression of social behaviors.

One such circuit is the vertebrate social behavior network (SBN). This includes the lateral septum (LS), bed nucleus of the stria terminalis (BNST), medial preoptic area (mPOA), paraventricular (PVN), anterior (AH), and ventromedial (VMH) hypothalamic nuclei, the ventral tegmental area (VTA) and periaqueductal gray (PAG) (Newman, 1999; Goodson, 2005; Goodson and Kingsbury, 2013). Rather than an exhaustive list of regions that facilitate social processes (Rogers-Carter and Christianson, 2019), the SBN is an evolutionarily conserved suite of nuclei responsible for interpreting and generating responses to social stimuli (Goodson, 2005; O'Connell and Hofmann, 2012). SBN nuclei or "nodes" are differentially engaged during specific behaviors (Lin et al., 2011; Lee et al., 2014; Decot et al., 2017; McHenry et al., 2017; Kohl et al., 2018; Tschida et al., 2019); however, coordinated patterns of activity or functional connectivity (Friston, 2011) across the SBN contribute to variation in behavioral output (Goodson, 2005; Goodson and Kabelik, 2009).

Since the original proposal of the SBN (Newman, 1999), analytical tools have been developed to quantitatively describe functional anatomical networks (Sporns, 2010; Fornito et al., 2016). For example, metrics such as density measure functional connectivity in a given network, whereas the clustering coefficient is an indicator of "small-world" networks which display increased efficacy of communication among regions (Watts

and Strogatz, 1998). Community structure/modularity calculates the degree to which nodes assemble into functionally similar clusters (Newman and Girvan, 2004). Functional networks are disrupted in human psychopathologies (Bullmore et al., 1997; van den Heuvel and Sporns, 2019), emphasizing the importance of investigating network-level features in rodent translational models (Van den Heuvel et al., 2016). Network-based analyses in non-traditional model systems describe changes in SBN functional connectivity following presentation of socially salient vocal stimuli (Hoke et al., 2005; Ghahramani et al., 2018); however, no such studies exist in laboratory mice.

Murine vocalizations are a source of context-dependent information during social interactions (Hanson and Hurley, 2012; Finton et al., 2017; Warren et al., 2018; Sangiamo et al., 2020; Warren et al., 2020). Vocal processing relies on auditory circuitry as well as functionally diverse nuclei such as the SBN. For example, receivers must extract the physical characteristics of vocal signals (e.g., frequency, duration, amplitude, etc.) and interpret them in light of their own experiences and current conditions (Petersen and Hurley, 2017). Investigating whether social isolation disrupts vocal processing in circuits such as the SBN will be important in understanding the mechanisms underlying aberrant behavior in mouse models of communicative and affective disorders (Portfors and Perkel, 2014).

Serotonergic signaling is sensitive to social isolation: socially isolated mice downregulate 5-HT receptor expression in hypothalamic nodes of the SBN (Schiller et al., 2003; Bibancos et al., 2007). As anatomically distinct regions of the dorsal raphe nucleus

send serotonergic projections to the SBN (Schwarz et al., 2015; Muzerelle et al., 2016; Beier et al., 2019), serotonin may modulate SBN activity in accordance with an animal's internal state and changes in the external environment (Muzerelle et al., 2016; Niederkofler et al., 2016; Ren et al., 2018). Broadly activating serotonergic pathways affects neural activity markers across a distributed suite of nuclei including the SBN (Giorgi et al., 2017; Grandjean et al., 2019); however, it remains unknown whether social experience interacts with serotonin signaling to affect activity-dependent measures and network-level metrics such as functional connectivity.

We use immediate early gene (IEG) mapping to test the hypothesis that serotonin signaling interacts with social experience to affect patterns of cFos-ir neurons in the SBN of male mice following presentation of female broadband vocalizations. Increasing available serotonin increased the IEG response in several SBN nodes. This effect was more prominent in socially isolated mice regardless of drug treatment. Despite increases in cFos-ir neurons, network analyses reveal fewer functional relationships within the SBN of socially isolated mice.

Materials and methods

Animal information

The [Author University] Institutional Animal Care and Use Committee (Protocol #15-021) approved all of the following experiments. Individual cohorts of male CBA/J mice (*Mus musculus)* from different litters were shipped from Jackson Laboratories (Bar Harbor,

ME, USA) and received at 18 – 24 days of age (Fig. 1a). Each cohort was assigned to 1 of 3 pharmacological treatment groups: saline (control), fenfluramine, or pCPA (see pharmacological details below). Upon arrival, mice were separated into either social housing of 3 mice per cage or into isolated housing (Fig. 1b). Mice remained in social (SOC) or isolated (ISO) conditions on a 14:10 light/dark cycle with *ad libitum* access to food and water and weekly cage changes for 28 – 30 days prior to vocal playback (Fig. 1c – d). ISO mice were physically separated from conspecifics; however, all experimental animals were housed in the same room within our vivarium. While ISO mice were potentially exposed to olfactory, auditory, and/or visual stimuli from neighboring cages, similar conditions did not attenuate the effects of social isolation in other studies (Keesom et al., 2017b; Keesom et al., 2017a; Manouze et al., 2019).

Pharmacology

pCPA methyl ester hydrochloride (pCPA; 4-Chloro-DL-Phenylalanine methyl ester hydrochloride, Tocris, Minneapolis, MN, USA) was used to deplete systemic serotonin. pCPA is a non-reversible inhibitor of tryptophan hydroxylase (TPH; the rate-limiting enzyme in serotonin synthesis) (Koe et al., 1966). Over the course of 3 – 4 days, pCPA depletes serotonin in brain regions including the hippocampus, striatum, and cortex (Dailly et al., 2006). Conversely, Dexfenfluramine hydrochloride (Fenluramine; (S)-N-Ethyl-α-methyl-3-(trifluoromethyl) benzeneethanamine hydrochloride; Tocris), which releases stores of vesicular serotonin and blocks its reuptake at the synapse (Davis and

196 Faulds, 1996; Rothman and Baumann, 2002), was used to acutely increase levels of
197 available serotonin.
198
199 Fenfluramine (FEN) and pCPA were diluted in 0.9% sterile saline within 3 days of
200 use. pCPA was administered at 200mg/kg in a volume of 5mL/kg; FEN was administered
201 at 100mg/kg in a volume of 5mL/kg (Hanson and Hurley, 2016). Sterile saline (vehicle;
202 10mL/kg) was used for all control injections. Each mouse in SOC cages received the
203 same pharmacological treatment. Injections were administered interperitoneally following
204 brief anesthetization with isoflurane, after which mice were returned to their home cage.
205 Beginning 3 days prior to playback, mice were transferred from housing quarters to the
206 experimental room where they received injections at roughly 24-hour intervals in the
207 morning. Over the course of these 3 days, pCPA mice received pCPA injections while
208 FEN and saline (SAL) mice received equivalent injections of sterile saline (Fig. 1d).
209 Following injections, mice remained in the experimental room for 45 minutes before being
210 returned to the vivarium. This process was designed to habituate mice to injections and
211 being moved between rooms in order to reduce non-specific cFos expression prior to
212 playback trials. On the day of playback, pCPA and SAL mice were injected with sterile
213 saline 45 minutes prior to trials. FEN mice received FEN injections 45 minutes prior to
214 playback (Fig. 1e). For each treatment group n = 9 except for SOC-SAL, where n = 8.
215 Over the course of injections, ISO-pCPA mice lost a significant amount of weight (paired
216 $t_8 = 2.82$, $p < 0.05$, mean difference 0.43g $\pm$ 0.15g), but there was no difference between
217 the weights of treatment groups on the day of playback ($p = 0.2$).
218

Playback trials

Ninety minutes before playback trials, mice were retrieved from animal quarters and placed in a quiet room. After 45 minutes, the first of three animals received an injection (as above) and was returned to its home cage (Fig. 1e). Forty-five minutes post injection, focal mice were transferred from their home cage to an identical testing cage (12x6x6 inches) with fresh bedding within in a sound attenuation chamber (Coulbourn Habitest, Whitehall, PA, USA) with an ultrasonic speaker (Ultrasonic Dynamic Speaker Vifa, Avisoft Bioacoustics, Glienicke/Nordbahn, Germany) powered by an UltraSoundGate Player 116 (Avisoft Bioacoustics). Trials were monitored with a CCD video camera (30 fps) placed above the test cage, with SuperDVR software (Q-See, Digital Peripheral Solutions Inc.) and a Q-see 4 channel DVR PCI video capture card. Trials were 60 minutes and playback consisted of 14 – 15 naturalistic bursts of 5 female broadband vocalizations (BBVs; Fig. 1f); the final number of BBVs (70-75) represented the average number of BBVs emitted during the study from which they were recorded. All mice were played back the same BBV sound file; omission of the final burst of 5 BBVs was counterbalanced across groups. Following trials, spectrograms of the playback were created in Avisoft, and the number of male-emitted ultrasonic vocalizations were quantified.

Playback generation

241 Source BBVs were originally recorded during sociosexual interactions between
242 male and female CBA/J mice. First, spectrograms of sociosexual interactions were
243 generated using Avisoft SASlab Pro software; next, individual female BBVs were located,
244 high-pass filtered to remove any potentially overlapping male ultrasonic vocalizations, and
245 copied into a new playback audio file. We assembled naturalistic bursts of 5 individual
246 BBVs and interspersed 270 seconds of silence between bursts. BBVs were calibrated by
247 matching rms intensity of the playback (as recorded in the testing arena) to the intensity
248 of the originally recorded vocalizations. The same condenser microphone (CM16/CMPA,
249 Avisoft Bioacoustics) with an UltraSoundGate 116Hb sound card (250 kHz sample rate
250 Avisoft Bioacoustics) was used to assess the intensities of the originally recorded
251 vocalizations and the playback.
252
253 In naturalistic social interactions, female BBVs correlate with male-directed
254 aggression (i.e., rejection-like behaviors); as they also emitted during mounting, BBVs
255 are considered to be functionally ambiguous (Finton et al., 2017). Our playback file
256 consisted of BBVs that were acquired during multiple interactions where mounting either
257 did or did not occur. Thus, any potential structural differences in BBVs emitted during
258 different contexts (i.e., mounting vs. rejection) would not shape the overall valence of
259 playback.
260
261 *Immunohistochemistry*
262

Playback lasted for 60 minutes, at which point focal animals remained in the sound attenuation chamber for 30 additional minutes to allow for accumulation of the cFos protein (Kovacs, 2008). Ninety minutes following the onset of playback, mice were deeply anesthetized with isoflurane and transcardially perfused with ice-cold Krebs-Henseleit solution (pH 7.2) followed by 50mL of 4% paraformaldehyde in phosphate buffer (PFA). Brains were extracted and post-fixed overnight in PFA, transferred to 30% sucrose in phosphate buffered saline (PBS; pH 7.4) for ~48 hours, and cut into 3 series of 50µM sections in the coronal plane using a freezing microtome. Sections were collected throughout the rostral-to-caudal extent of the inferior colliculus (IC; approximately Bregma -5.34mm thru -4.36mm) and starting at the appearance of the median eminence (Bregma -1.94mm) through the bifurcation of the anterior commissure (AC; ~ Bregma +0.38mm). Sections were stored in cryoprotectant solution at -80°C until immunohistochemistry (IHC). Three separate IHC runs counterbalanced across treatment groups were performed as follows.

Tissue was equilibrated to room temperature; free-floating sections were first sorted in PBS, then washed for 5x5 minutes in PBS, followed by a 1-hour soak in blocking solution: PBS + 10% donkey serum (DS; Millipore, Burlington, MA, USA) and 0.3% Triton-X100 (Tx; Millipore). Sections were incubated for 18 hours at room temperature in rabbit anti-cFos (F7799, Lot:105M4831V; Sigma-Aldrich, St. Louis, MO) diluted 1:2000 in PBS + 5% DS and 0.3% Tx (diluent). Following primary incubation, sections were washed 4x5 minutes in PBS + 0.5% DS, and then incubated for 2 hours at room temperature in AlexaFluor donkey anti-rabbit 680 (Life Technologies, Carlsbad, Calif., USA) diluted

6:1000 in diluent. Sections were washed 3x10 minutes in PBS, followed by a 30-minute incubation in NeuroTrace™ 500/525 Green Fluorescent Nissl (NT) diluted 1:200 in PBS. Following a final, 10-minute PBS wash, sections were mounted onto chrome alum-subbed slides and cover-slipped with Prolong Gold Antifade Reagent with DAPI (4,6-diamidino-2-phenylindole; Life Technologies) and stored at 4°C until microscopy.

Image acquisition and anatomy

All images were collected at 10X with 568nm resolution using a Leica SP8 scanning confocal microscope. cFos immunoreactive (-ir) neurons were visualized using a 680nm laser line; DAPI and NT were visualized using 405nm and 490nm laser lines respectively. The intensity of each laser line was identical for all images, and tissue was scanned at 12 separate z planes spaced 2.41uM apart. When >1 confocal image was needed to capture the expanse of a nucleus (LS, mPOA, VMH, PAG) or adjacent nuclei (i.e., PVN and AH), images were automatically merged using Leica Application Suite X software (Leica Microsystems, Wetzlar, Germany). In instances where tissue was damaged, the next available section was used.

SBN regions were identified based on cytoarchitecture at approximate rostral-caudal levels relative to Bregma as per the mouse brain atlas (Paxinos and Franklin, 2004). The LS (Fig. 1G) was collected beginning at the bifurcation of the anterior commissure (ac; Bregma 0.38mm) and continued for three consecutive sections. We captured the medial division of the BNST starting at the level where the bifurcation of AC begins to close (Bregma 0.26mm). BNST (Fig. 1H) was sampled bilaterally in two

consecutive sections within boundaries established by the lateral ventricle and the stria terminalis (lateral), the fornix (medial), and ventrally by the anterior commissure. Sampling for mPOA (Fig. 1I) began at the closure of AC (Bregma 0.14mm) and continued for two consecutive sections. PVN was shot at three consecutive sections beginning at the appearance of a triangular cluster of neurons immediately adjacent to the dorsal aspect of the third ventricle (Bregma -0.70mm). We collected AH beginning at the second level of PVN (Fig. 1J; Bregma -0.82mm) and continued for 3 consecutive sections. The final level of AH overlapped with the first section where sampling for VMH began (Bregma -1.22) and continued for 2 – 3 sections (Fig. 1K). PAG (Fig. 1L) was collected for three consecutive sections beginning approximately at Bregma -4.24mm.

Z stacks for laser lines 405 (DAPI), 490 (NT), and 680 (cFos-ir) were projected using the maximal intensity function in Fiji (National Institute of Health, Bethesda, MD, USA) (Schindelin et al., 2012), and saved as .tif files prior to analysis. A single observer blind to animal identity and treatment group performed all image analyses and microscopy.

Cell counting

Regions of interest (ROI) were drawn around the boundaries of SBN nodes based on cytoarchitecture (Fig. 1G – L) and saved using the Fiji ROI manager. cFos-ir neurons were quantified using custom macros in ImageJ as follows. First, background was subtracted from cFos images using the rolling ball function with a radius of 50 pixels. ROIs derived from NT images were transferred to the corresponding cFos channel. Using the

internal clipboard function, we created a new image containing only the selected ROI. Tsai's moments threshold was applied using Fiji's Auto Threshold plugin v1.17. The thresholded image was then made binary, the watershed function was applied, and the analyze particles function was run thresholding out objects with fewer than 75 pixels and a circularity < 0.15. Cell counts were normalized by multiplying the total number of cFos-ir neurons in each region by 100 divided by the sum of the areas of the ROI(s) from which they were obtained.

Statistics

Inferential statistics were performed in JMP Pro® Version 14 (SAS Institute, Inc. Cary, NC, USA) with an $\alpha = 0.05$, or GraphPad Prism version 8 (La Jolla, CA, USA). We used repeated measures multivariate analysis of variance (MANOVA) to test the between-subject effects of housing (SOC vs. ISO) and drug treatment (SAL vs. FEN vs. pCPA) on the within-subjects measure of cFos-ir neurons/100μm^2 across 7 nodes of the SBN. We found main effects of housing and drug treatment, as well as a significant housing-by-drug interaction (see results). We followed MANOVA with a series of linear mixed model analyses with housing and drug treatment as fixed effects to test for group differences in cFos-ir neurons within each SBN node. Our model included IHC run as a random effect to control for potential variation introduced by separate IHC procedures. As SOC mice were housed in groups of 3, we also included cage as a random effect to control for potential within-cage influence on cFos expression. *Post hoc* differences between groups were assessed via independent t tests where applicable.

Next, we performed pair-wise correlations on the number of cFos-ir neurons to test for functional relationships between SBN nodes within each of our 6 treatment groups. P values obtained from Pearson coefficients were corrected for multiple comparisons using the two-stage linear step-up procedure of Benjamini, Krieger and Yekutieli (Benjamini et al., 2006). To test for differences in the distribution of inter-nodal correlations between groups, we performed principal components analysis (PCA) on the covariation matrix derived from these data.

Network analyses were performed on within-group correlations using Gephi open source network analysis and visualization software version 0.9.2 (Bastian et al., 2009). Functional relationships were visualized as unweighted, undirected graphs using the ForceAtlas2 algorithm, which spatially distributes nodes based on the overall strengths of each node's correlations (Bastian et al., 2009; Jacomy et al., 2014). Graphs were subsequently filtered so that non-significant edges (i.e., correlations $p > 0.05$) were excluded from visualization. The overall relatedness of any given region is indicated not only by its shared edges, but by its position relative to other nodes. In order to quantitatively describe functional relationships among groups, we performed 3 separate graph analyses in Gephi: First, we calculated network density, the number of significant intraregional correlations as a proportion of the total number of possible correlations, for each treatment group. This analysis, a graph-based supplement to our strength of correlation analysis (see results), quantifies the overall functional connectivity of the SBN in each treatment group. Next, for each treatment group we calculated the average clustering coefficient as the likelihood for any pair of a node's functional connected

neighbors to be connected to each other (Watts and Strogatz, 1998; Fornito et al., 2016). Finally, we performed community analysis which parses nodes into highly interconnected subgroups which is indicative of functional commonality (Fornito et al., 2016).

Results

Repeated measures MANOVA found significant effects of housing ($F_{6,36} = 4.45$, $p = 0.002$) and drug treatment ($F_{12,74} = 5.71$, $p < 0.0001$), as well as a significant housing-by-drug interaction ($F_{12,74} = 3.17$, $p = 0.001$) on number of cFos-ir neurons/100μm^2 across 7 nodes of the SBN. Next, we performed linear mixed model analyses with housing and drug treatment as fixed factors, controlling for random effects of IHC run and cage. Below we report only p values for linear mixed models; a complete summary can be found in Table 1. Arithmetic means for housing and drug treatments are reported in Table 2a and 2b respectively. Results from the applicable *post-hoc* comparisons can be found in extended data Figure 2-1.

Our model detected effects of housing in the BNST ($p = 0.017$), mPOA ($p = 0.018$), PVN ($p = 0.005$), and PAG ($p = 0.021$). ISO mice had higher numbers of cFos-ir neurons in each one of these regions (Tukey's HSD, $p \leq 0.02$). We found significant effects of drug treatment in LS ($p < 0.0001$; Fig 2A), BNST ($p < 0.0001$; Fig 2B), mPOA ($p < 0.0001$; Fig 2C), PVN ($p < 0.0001$; Fig 2D), AH ($p = 0.006$; Fig 2E), VMH ($p = 0.0001$; Fig 2F). In each region except for AH, FEN mice had significantly more cFos-ir neurons than both SAL and pCPA mice (Tukey's HSD, $p \leq 0.0007$). In AH, FEN mice had significantly more cFos-

401 ir neurons than pCPA mice (Tukey's HSD, p = 0.005), and a trend towards an increase
402 relative to SAL mice (Tukey's HSD, p = 0.054). Interestingly, PAG was the only region
403 where our model did not detect a significant effect of drug treatment (p > 0.4; Fig 2G).
404 Drug effects were dependent upon housing conditions as indicated by significant
405 interaction terms in LS (p = 0.018) and PVN (p = 0.003). In LS, the interaction is driven
406 by an increase in cFos-ir neurons in ISO-pCPA compared to the SOC-pCPA mice. In
407 PVN, the interaction is driven by an almost 2-fold increase in cFos-ir neurons in ISO-FEN
408 compared to SOC-FEN mice.
409
410 We found a main effect of housing ($F_{1,47}$ = 5.97, p = 0.02) and a significant housing-
411 by-drug interaction ($F_{2,47}$ = 6.03, p = 0.005; data not shown) on the number of ultrasonic
412 vocalizations (USVs) emitted by focal males during playback. The interaction was driven
413 by a significant increase in USV production in ISO-SAL compared to SOC-SAL mice
414 (Tukey's HSD, p = 0.004). There were no differences in USV production between SOC
415 and ISO males in either the FEN or pCPA groups (p > 0.8). Interestingly, there were no
416 relationship between USV production and cFos-ir within the SBN of any treatment group.
417
418 As the SBN comprises a reciprocally connected anatomical network (Hahn et al.,
419 2019), we tested whether correlations of neural activity markers between nodes (i.e.,
420 functional connectivity) varied between treatment groups. Figure 3 summarizes these
421 data as heatmap matrices based on the Pearson r values of each pairwise correlation. A
422 detailed summary of pairwise correlations of cFos-ir neurons between SBN nodes within
423 each of our 6 treatment groups can be found in extended data figure 3-1. Cursory analysis

of the heatmaps suggested that SOC-FEN (Fig 3b) and SOC-pCPA (Fig 3c) had more relatively strong correlations (i.e., more functional connectivity) than all other treatment groups. To test this, we used two-way ANOVAs on the absolute value of Pearson r scores of each treatment group (Tanimizu et al., 2017). We found a main effect of housing ($F_{1,120}$ = 6.33, p = 0.013; Fig, 3g), where SOC mice had larger Pearson r values than ISO mice (Tukey's HSD, p = 0.013). Drug treatment ($F_{2,120}$ = 2.68, p = 0.07) and housing-by-drug interaction ($F_{2,120}$ = 2.45, p = 0.09) approached but did not reach statistical significance.

While we did not find a statistically significant effect of drug treatment on the strength of inter-node correlations, we hypothesized that pharmacologically increasing or systemically depleting available serotonin would differentially affect the distribution of functional relationships. We thus performed PCA on the covariation matrix generated by cFos-ir counts. PC1 had an eigenvector of 543.53 which accounted for over 76% of the variation and contained eigenvalues most strongly loaded by mPOA (0.682) and PVN (0.553; Fig. 3H). We analyzed PC1 scores between groups via 2-way ANOVA and found main effects of housing ($F_{1,41}$ = 14.11, p < 0.001) and drug treatment ($F_{2,41}$ = 39.28, p < 0.0001; Fig. 3I), but no significant interaction ($F_{2,41}$ = 2.43, p = 0.10). FEN mice had divergent and significantly different (Tukey's HSD, p < 0.0001) PC1 scores from both SAL and FEN mice; Thus, despite having similar overall Pearson r values, the distribution of correlations among SBN nodes was different between drug treatment groups.

We visualized the distributions of correlations using the ForceAtlas2 algorithm in Gephi, and filtered the resulting graphs to exclude non-significant edges (i.e., correlations

447 $p > 0.05$) from visualization (Bastian et al., 2009; Jacomy et al., 2014). There were visible
448 differences between groups in functional network structure: ISO mice have fewer
449 significant functional relationships than SOC mice, which is indicated by relatively few
450 connections between nodes (Fig. 4A – F). For example, cFos-ir neurons in the PVN of
451 ISO-FEN mice is significantly correlated with AH; thus, PVN shares an edge with only AH
452 (Fig. 4E). Conversely, in SOC-FEN mice the number of cFos-ir neurons in the PVN is
453 significantly correlated with LS, BNST, mPOA, AH, and PAG; thus, PVN shares edges
454 with each of these regions (Fig. 4B). Further, the strength of functional relationships is
455 indicated by the closeness of nodes in space. In SOC-pCPA mice, the significant
456 correlation between cFos-ir in mPOA and BNST is indicated not only by a shared edge,
457 but their relative adjacency (closeness) in space (Fig. 4C). In ISO-pCPA mice, there was
458 a relatively weak, non-significant correlation between cFos-ir in mPOA and BNST which
459 is reflected by a relatively large distance between these nodes in space (Fig. 5f).
460
461 We quantifiably described the network organization of the above graphs by
462 performing three separate graph analyses. First, we quantified the number of significant
463 functional relationships as a proportion of total possible functional relationships (i.e.,
464 functional density) (Fornito et al., 2016). In each of the three SOC treatment groups, there
465 was an over twofold increase in functional density compared to their ISO counterparts
466 (Fig. 4G). While increased density indicates that there is more functional connectivity
467 between regions in SOC mice, this metric tells us little about the nature of these
468 correlations (Bullmore and Sporns, 2009). Importantly, do correlated nodes go on to form
469 a) additional functional relationships, and/or b) larger functional modules?

Next, we calculated the clustering coefficient, the average number of connected pairs of a node's connected neighbors of each treatment group. SOC mice had higher clustering coefficients than ISO mice in each treatment group (Fig. 4H). Indeed, regardless of drug treatment, ISO mice had a clustering coefficient of zero; thus, even when ISO mice have significant correlations between nodes, those regions do not in-turn form additional connections with each other. Our final graph analysis assessed modularity/community structure in SOC and ISO mice. In community structure analysis, the smallest number of communities that can be formed is one, indicating a completely connected group; the maximum number of communities is equal to the number of nodes contained in the analysis, and indicates complete functional segregation. We found that ISO mice formed more communities than their socially reared counterparts in each of the drug treatment groups (Fig. 4I). Together, our results support that functional networks are more disconnected in ISO mice.

Discussion

Individual experience establishes the backdrop upon which current events are interpreted. Early-life social isolation can profoundly affect an animal's behavioral phenotype (Mumtaz et al., 2018), and likely affects how social signals (e.g., vocalizations) are represented in the brain; however, the effects of social isolation on the neural response to rodent vocalizations are relatively unexplored. We tested whether social experience interacts with serotonin signaling to affect IEG expression in the male SBN following playback of female BBVs. Fenfluramine robustly increased the number of cFos-

493 ir neurons across all nodes of the SBN except PAG. Housing treatment also affected IEG
494 induction: ISO mice had more cFos-ir neurons in several nodes of the SBN than SOC
495 mice. Despite a generalized increase in cFos-ir, ISO mice had lower functional
496 connectivity among regions than SOC mice. Indeed, functional density, clustering, and
497 community structure remained relatively low in SOC mice despite pharmacological
498 changes in available serotonin. Importantly, drug treatment had little effect on graph
499 analyses in ISO mice and facilitated network measures in SOC mice.
500
501 *Social experience interacts with serotonin signaling to affect neural responses in the SBN*
502
503 IEG mapping has established that early-life stressors alter neural activity markers
504 at the level of individual SBN nodes. Chronic social subjugation decreased cFos
505 expression in the LS, PVN, and PAG following open-arm exposure in male mice
506 (Singewald et al., 2009). In rats, post-weaning social isolation increased both aggression
507 and cFos-ir neurons in the BNST and PVN (but not LS or PAG) following a resident-
508 intruder paradigm (Toth et al., 2012). Despite structural interconnectedness, we found
509 that changes in the cFos response in the SBN of ISO mice was not global: BNST, mPOA,
510 PVN, VMH, and PAG had increased cFos-ir neurons, whereas LS and AH did not.
511 Interestingly, the direction (i.e., an increase) of the cFos response was similar in each
512 region affected in ISO mice.
513
514 The effects of housing on cFos-ir neurons were modulated by drug treatment.
515 Similar to previous studies (Li and Rowland, 1993), we found that fenfluramine increased

cFos-ir neurons in all nodes of the SBN except for PAG. However, the effects of fenfluramine were not homogenous across housing treatments: cFos-ir neurons were increased to a greater extent in the PVN and mPOA of ISO-FEN compared to SOC-FEN mice (Fig 3C – D). Conversely, we found no difference in cFos-ir in the PVN of pCPA mice regardless of social experience, an observation consistent with previous studies in rats (Harbuz et al., 1993; Conde et al., 1998). Serotonin affects neural activity through a combination of excitatory and inhibitory serotonin receptor (5-HTR) subtypes (Barnes and Sharp, 1999), and 5-HTR expression patterns are sensitive to social isolation (Schiller et al., 2003; Bibancos et al., 2007); thus, the net effect of serotonergic manipulations is likely driven by complex excitatory and inhibitory interactions within and between each node of the SBN. Importantly, the increase in cFos-ir neurons was not observed exclusively in ISO-FEN mice: ISO-pCPA mice had more cFos-ir neurons in LS, BNST, mPOA, and PAG than SOC-pCPA mice.

Together, we found heterogenous effects of both pharmacology and housing conditions on the number of cFos-ir neurons within nodes of the SBN. An *a priori* assumption is that the SBN is a structurally interconnected network within which the patterns of functional connectivity are indicative of behavioral context (Newman, 1999; Goodson, 2005; Goodson and Kabelik, 2009). We therefore tested whether functional network measures differed within the SBN of SOC or ISO mice.

Social experience affects functional connectivity in the SBN

The term functional connectivity, defined as "statistical dependencies among remote neurophysiological events" (Friston, 2011), has been used extensively in human fMRI studies to describe activity patterns in resting and pathological states. This statistical phenomenon appears to be a crucial component to adaptive social processes across multiple species, including humans (Lynall et al., 2010). Immediate early gene mapping in non-traditional vertebrate model systems demonstrates functional connectivity between neuromodulatory systems/circuits (including the SBN) during vocal-acoustic processing in fishes (Petersen et al., 2013; Ghahramani et al., 2018) and frogs (Hoke et al., 2005), as well as prosocial and aggressive behavior in fishes (Weitekamp and Hofmann, 2017; Butler et al., 2018) and lizards (Kabelik et al., 2018). In male prairie voles (*Microtus ochrogaster*), oxytocin receptor antagonists reduce functional connectivity within the SBN and attenuate partner preference behavior (Johnson et al., 2015). In mice, Tanimizu et al. (2017) demonstrated that functional connectivity between memory-associated regions (including nodes of the SBN) was increased following a social learning task. Finally, different clusters of functional relationships in the SBN are observed in subordinate mice who maintain their beta status compared to those who ascend through the social hierarchy (Williamson et al., 2019).

We found that functional connectivity was decreased in ISO relative to SOC mice following playback of female BBVs. Importantly, these results were not due to a global increase in IEG induction as ISO mice tended to have more cFos-ir neurons than SOC mice. That functional connectivity is disrupted in the SBN of ISO mice represents an important foundation from which to develop models of how variation in functional network

562 architecture relates to variation in aberrant behavioral (Keesom et al., 2017b; Manouze
563 et al., 2019) and neural phenotypes (Keesom et al., 2017a; Keesom et al., 2018) following
564 early-life social stress.
565
566 We further analyzed patterns of functional connectivity by PCA and found that FEN
567 mice had positive average PC1 scores, whereas SAL and pCPA mice had negative
568 values (Fig. 4i). Thus, variation in the distribution of functional relationships differs
569 following acutely increasing (i.e., with FEN) or systemically depleting (i.e., with pCPA)
570 serotonin. Interestingly, the general direction of these relationships was consistent *within*
571 drug treatment regardless of housing conditions. Therefore, while overall functional
572 connectivity may be preferentially modulated by social experience, serotonin signaling
573 drives variation in the nodes that are functionally coupled. However, the extent to which
574 the effects of social experience and serotonin signaling are independent of each other
575 remains unknown.
576
577 *Individual nodes disproportionately affect functional connectivity*
578
579 PCA revealed that individual nodes disproportionately affect variation in functional
580 connectivity. We found that eigenvectors within PC1 were most heavily loaded by mPOA
581 and PVN. As mPOA and PVN underlie different functions, they may also drive variation
582 in circuit-level metrics in different manners. mPOA has increased IEG induction following
583 playback of social vocalizations in frogs and songbirds (Hoke et al., 2005; Maney et al.,
584 2008); in mice, mPOA is a crucial site for affective-olfactory integration (Dhungel et al.,

2011; McHenry et al., 2017), and activity in mPOA coincides with sociosexual investigation and facilitates mounting behavior (Wei et al., 2018). As the behavioral response to vocal signals (i.e., BBVs) is modulated by olfactory stimuli (Grimsley et al., 2013; Seagraves et al., 2016; Ronald et al., 2020), mPOA is in a functional anatomical position to integrate multisensory stimuli and effect circuit-level responses to vocal signals (Kohl et al., 2018). However, to our knowledge no studies have directly investigated mPOA involvement in rodent vocal processing.

We found that the number of cFos-ir neurons in the PVN is not only increased in ISO mice, but contributes a significant amount of variation to functional relationships within the SBN. Within the PVN, dysregulation of corticotropin-releasing factor (CRF) neurons which modulate the hypothalamic-pituitary-adrenal axis contributes to cardiovascular disease and impaired immune function in animal models of chronic social isolation as well as in persons with early-life social trauma (Heim and Nemeroff, 2001; McEwen, 2003; Cacioppo et al., 2015). Further, chemically heterogeneous PVN neurons underly different suites of behaviors: activating CRF neurons in PVN drives conditioned place aversion (Kim et al., 2019), whereas activating oxytocin neurons drives pup retrieval behavior in response to ultrasonic vocalizations (Marlin et al., 2015). Elucidating the chemical phenotypes and projection profiles of isolation-sensitive neurons in the PVN (and SBN in general) will be crucial to understanding the mechanisms through which different nodes affect functional relationships within the SBN.

Network measures are lower in ISO relative to SOC mice

608 Variation in functional relationships includes reduced functional connectivity in ISO
609 mice. Further, we found decreased network density and clustering in ISO mice, which is
610 consistent with observations that similar reductions are observed in persons with
611 schizophrenia (Lynall et al., 2010) and depression (Wise et al., 2017). Similarly, functional
612 dysconnectivity within the SBN may provide a partial mechanism for decreased social
613 competence observed in mice raised in social isolation (Keesom et al., 2017b).
614 Investigating the mechanisms that drive variation in functional dysconnectivity will
615 contribute to a better understanding of the diverse array of physiological and behavioral
616 consequences observed in animals following social isolation and other early-life stressors
617 (Heim and Nemeroff, 2001; Mumtaz et al., 2018). As neither FEN nor pCPA were
618 sufficient to facilitate an increase in network measures in ISO mice, it is critically important
619 to consider variation in an individual's contextual state (i.e., social history, physiological
620 condition, pathological severity, etc.,) when designing experiments and interpreting the
621 results of psychoactive reagents on animal or human subjects (Bartz et al., 2011).
622
623 Technical considerations
624
625 This study does not directly compare the cFos response in the SBN following
626 playback of BBVs to a non-social acoustic stimulus (i.e., pure tones) or a silent condition.
627 Playback of social vocalizations is sufficient to increase the cFos expression relative to
628 tones in in the PAG of rats (Ouda et al., 2016), and relative to ambient environmental
629 noise in multiple SBN nodes in the midshipman fish (*Porichthys notatus)* (Petersen et al.,
630 2013; Ghahramani et al., 2018). However, a lack of playback in the current study would

not necessarily be a behaviorally neutral condition, given that silence could have a very different significance for socially housed versus isolated males. Likewise, mouse vocal signals encompass a wide range of frequencies and nonlinear structures (Holy and Guo 2005; Lupanova and Egorova 2015; Grimsley et al. 2016; Finton et al. 2017, Niemczura et al. 2020) and some commonly used 'control' sounds can evoke behavioral responses similar to call playback (Hood et al. in preparation). In comparison to silence or other non-vocal sounds, playback of BBVs is a condition with a behavioral salience that is relatively well-understood. BBVs correspond to fewer male mounts of females in observational studies (Finton et al. 2017). Playback of BBVs alters the number of USVs as well as the numbers of males making USVs (Ronald et al. 2020; Niemczura et al. 2020; Hood et al. in preparation). BBVs are therefore suppressive to some types of social behaviors, creating a defined behavioral context in the current study. However, we are unable to determine whether the observed cFos response in the SBN of SOC and ISO mice is selective for BBVs (Maney et al., 2006; Maney et al., 2008), whether functional connectivity is an emergent response to socially salient stimuli (Hoke et al., 2005; Ghahramani et al., 2018), or as a potential confound from a novel testing environment (VanElzakker et al., 2008) or as a direct result of social isolation in SOC animals (Matthews et al. 2016). Further studies are needed to directly test how the SBN responds to social vocalizations, and to probe the consequences of variation in functional connectivity in the production of murine social behaviors.

IEG mapping is limited in that there is no direct relationship with the production of action potentials and the presence of IEG products (including cFos) (Clayton, 2000;

Kovacs, 2008). Despite its wide use as a proxy for neural activation, the cFos protein is a transcription factor; one interpretation of our data is that instead of an increase in neural activity *per se,* we are observing an increased potential for neuroplasticity in ISO mice. Further, using cFos-ir as a putative marker for neural activity limits our temporal resolution to the entire 60-minute trial. It is therefore impossible to make causal or directional statements pertaining to functional connectivity. We make no assumption that functional relationships imply structural connectivity, or vice versa. For example, a subset of mPOA neurons monosynaptically project to PVN (Kohl et al., 2018); however, the particular neurons that connect mPOA and PVN might not be similarly engaged in our paradigm.

Importantly, because the presence of cFos-ir is an indicator of past neural activity, it may be robust to action potentials that otherwise habituate over the course of a repeated stimulus i.e., auditory playback. For example, whereas neurons in the inferior colliculus (IC) decrease spike rate following repeated presentation of auditory stimuli (Pérez-González et al., 2005), cFos-ir neurons are detectable in the IC following 90-minute playbacks of pure-tone stimuli (D'Alessandro and Harrison, 2014). Further, repeated presentation of ultrasonic distress calls increases cFos-ir within auditory and limbic structures in the rat (Ouda et al., 2016). We find it unlikely that the potential for SBN neurons to adapt to repeated playback of BBVs influenced our results. cFos takes approximately 30 minutes to reach detectable changes in expression, and the half-life of the cFos protein is approximately 45 minutes (Kovacs, 2008). The mice used in this study were at least 180 minutes removed from being transferred to the lab and 135 minutes

676 removed from injections; we would expect cFos induction brought on by these aspects of
677 our experimental design to be negligible.
678
679 Systemic pharmacological manipulations likely drive “off-target” effects such that
680 activity markers are influenced not only by serotonin signaling within the SBN, but via
681 direct or polysynaptic modulation of inputs into the SBN. Extrinsic to the SBN, depleting
682 systemic serotonin reduces synaptic densities in the cortex of rats (Chen et al. 1994) and
683 changes glutamate receptor distribution in the amygdala (Tran et al. 2013). Interestingly,
684 functional connectivity/density, clustering, and community structure remain relatively high
685 in SOC-FEN and SOC-pCPA mice despite potential “off-target” pharmacological and
686 physiological effects (Otchy et al., 2015) resulting from chronically depleting or acutely
687 increasing available serotonin. Manipulating site-specific serotonergic inputs into the SBN
688 will be crucial to untangling the effects of individual nodes on network-level functionality
689 (Ren et al., 2018). Importantly, network measures were also increased in SOC-SAL
690 relative to ISO-SAL mice suggesting the importance of social experience in the ability to
691 form functional relationships in the SBN.
692
693 **Conclusion**
694
695 Fenfluramine and social isolation each broadly increased cFos-ir within individual
696 nodes of the SBN following payback of social vocalizations. Importantly, by extending our
697 analyses from individual nodes to the network level, we found that functional connectivity,
698 clustering, and community structure within the SBN was highly dependent on social

699 experience, whereas patterns of functional connectivity (i.e., which nodes formed
700 functional relationships) were driven more by pharmacological manipulations. Our
701 findings suggest the hypothesis that functional dysconnectivity may underlie
702 psychopathological phenotypes that arise from social isolation and reinforces the
703 importance to move beyond functional analyses limited to individual nodes. We highlight
704 the importance of how laboratory housing conditions (SOC vs. ISO) can affect functional
705 neuroanatomical processes in rodents.

706 References

707

708 Bailey NW, Moore AJ (2018) Evolutionary Consequences of Social Isolation. Trends in
709 ecology & evolution.
710 Barnes NM, Sharp T (1999) A review of central 5-HT receptors and their function.
711 Neuropharmacology 38:1083-1152.
712 Bartz JA, Zaki J, Bolger N, Ochsner KN (2011) Social effects of oxytocin in humans:
713 context and person matter. Trends in cognitive sciences 15:301-309.
714 Bastian M, Heymann S, Jacomy M (2009) Gephi: an open source software for exploring
715 and manipulating networks. In: Third international AAAI conference on weblogs
716 and social media.
717 Beier KT, Gao XJ, Xie S, DeLoach KE, Malenka RC, Luo L (2019) Topological
718 Organization of Ventral Tegmental Area Connectivity Revealed by Viral-Genetic
719 Dissection of Input-Output Relations. Cell reports 26:159-167. e156.
720 Benjamini Y, Krieger AM, Yekutieli D (2006) Adaptive linear step-up procedures that
721 control the false discovery rate. Biometrika 93:491-507.
722 Bibancos T, Jardim D, Aneas I, Chiavegatto S (2007) Social isolation and expression of
723 serotonergic neurotransmission-related genes in several brain areas of male
724 mice. Genes, Brain and Behavior 6:529-539.
725 Bullmore E, Sporns O (2009) Complex brain networks: graph theoretical analysis of
726 structural and functional systems. Nature Reviews Neuroscience 10:186.
727 Bullmore E, Frangou S, Murray R (1997) The dysplastic net hypothesis: an integration
728 of developmental and dysconnectivity theories of schizophrenia. Schizophrenia
729 research 28:143-156.
730 Butler JM, Whitlow SM, Roberts DA, Maruska KP (2018) Neural and behavioural
731 correlates of repeated social defeat. Scientific reports 8:6818.
732 Cacioppo JT, Cacioppo S, Capitanio JP, Cole SW (2015) The neuroendocrinology of
733 social isolation. Annual review of psychology 66:733-767.
734 Chen, Ling, et al. "PCPA reduces both monoaminergic afferents and nonmonoaminergic
735 synapses in the cerebral cortex." Neuroscience research 19.1 (1994): 111-115.
736 Clayton DF (2000) The genomic action potential. Neurobiology of learning and memory
737 74:185-216.
738 Conde G, Renshaw D, Lightman S, Harbuz M (1998) Serotonin depletion does not alter
739 lipopolysaccharide-induced activation of the rat paraventricular nucleus. Journal
740 of endocrinology 156:245-252.
741 D'Alessandro LM, Harrison RV (2014) Excitatory and inhibitory tonotopic bands in
742 chinchilla inferior colliculus revealed by c-fos immuno-labeling. Hearing research
743 316:122-128.
744 Dailly E, Chenu F, Petit-Demoulière B, Bourin M (2006) Specificity and efficacy of
745 noradrenaline, serotonin depletion in discrete brain areas of Swiss mice by
746 neurotoxins. Journal of neuroscience methods 150:111-115.
747 Davis R, Faulds D (1996) Dexfenfluramine. Drugs 52:696-724.
748 Decot HK, Namboodiri VM, Gao W, McHenry JA, Jennings JH, Lee S-H, Kantak PA,
749 Kao Y-CJ, Das M, Witten IBJN (2017) Coordination of brain-wide activity
750 dynamics by dopaminergic neurons. 42:615.

751 Dhungel S, Urakawa S, Kondo Y, Sakuma Y (2011) Olfactory preference in the male rat
752 depends on multiple chemosensory inputs converging on the preoptic area.
753 Hormones and behavior 59:193-199.
754 Dolen G, Darvishzadeh A, Huang KW, Malenka RC (2013) Social reward requires
755 coordinated activity of nucleus accumbens oxytocin and serotonin. Nature
756 501:179-184.
757 Finton CJ, Keesom SM, Hood KE, Hurley LM (2017) What's in a squeak? Female vocal
758 signals predict the sexual behaviour of male house mice during courtship. Animal
759 Behaviour 126:163-175.
760 Fornito A, Zalesky A, Bullmore E (2016) Fundamentals of brain network analysis:
761 Academic Press.
762 Friston K (2011) Functional and effective connectivity: a review. Brain connectivity 1:13-
763 36.
764 Ghahramani ZN, Timothy M, Varughese J, Sisneros JA, Forlano PM (2018)
765 Dopaminergic neurons are preferentially responsive to advertisement calls and
766 co-active with social behavior network nuclei in sneaker male midshipman fish.
767 Brain research 1701:177-188.
768 Giorgi A, Migliarini S, Galbusera A, Maddaloni G, Mereu M, Margiani G, Gritti M, Landi
769 S, Trovato F, Bertozzi SM (2017) Brain-wide mapping of endogenous
770 serotonergic transmission via chemogenetic fMRI. Cell reports 21:910-918.
771 Goodson JL (2005) The vertebrate social behavior network: evolutionary themes and
772 variations. Hormones and Behavior 48:11-22.
773 Goodson JL (2013) Deconstructing sociality, social evolution and relevant nonapeptide
774 functions. Psychoneuroendocrinology 38:465-478.
775 Goodson JL, Wang Y (2006) Valence-sensitive neurons exhibit divergent functional
776 profiles in gregarious and asocial species. Proceedings of the National Academy
777 of Sciences of the United States of America 103:17013-17017.
778 Goodson JL, Kabelik D (2009) Dynamic limbic networks and social diversity in
779 vertebrates: from neural context to neuromodulatory patterning. Frontiers in
780 neuroendocrinology 30:429-441.
781 Goodson JL, Kingsbury MA (2013) What's in a name? Considerations of homologies
782 and nomenclature for vertebrate social behavior networks. Horm Behav 64:103-
783 112.
784 Grandjean J, Corcoba A, Kahn MC, Upton AL, Deneris ES, Seifritz E, Helmchen F,
785 Mann EO, Rudin M, Saab BJ (2019) A brain-wide functional map of the
786 serotonergic responses to acute stress and fluoxetine. Nature communications
787 10:350.
788 Grimsley JM, Hazlett EG, Wenstrup JJ (2013) Coding the meaning of sounds:
789 contextual modulation of auditory responses in the basolateral amygdala. The
790 Journal of neuroscience : the official journal of the Society for Neuroscience
791 33:17538-17548.
792 Hahn JD, Sporns O, Watts AG, Swanson LWJPotNAoS (2019) Macroscale intrinsic
793 network architecture of the hypothalamus.201819448.
794 Hanson J, Hurley L (2016) Serotonin, Estrus, and Social Context Influence c-Fos
795 Immunoreactivity in the Inferior Colliculus. Behavioral neuroscience.

796 Hanson JL, Hurley LM (2012) Female presence and estrous state influence mouse
797 ultrasonic courtship vocalizations. PloS one 7:e40782.
798 Harbuz MS, Chalmers J, De Souza L, Lightman SL (1993) Stress-induced activation of
799 CRF and c-fos mRNAs in the paraventricular nucleus are not affected by
800 serotonin depletion. Brain research 609:167-173.
801 Harlow HF, Dodsworth RO, Harlow MK (1965) Total social isolation in monkeys.
802 Proceedings of the National Academy of Sciences of the United States of
803 America 54:90.
804 Heim C, Nemeroff CB (2001) The role of childhood trauma in the neurobiology of mood
805 and anxiety disorders: preclinical and clinical studies. Biological psychiatry
806 49:1023-1039.
807 Hoke KL, Ryan MJ, Wilczynski W (2005) Social cues shift functional connectivity in the
808 hypothalamus. Proceedings of the National Academy of Sciences of the United
809 States of America 102:10712-10717.
810 Holy, T. E., Guo, Z. (2005). Ultrasonic songs of male mice. PLoS Biol, 3(12), e386.
811 Jacomy M, Venturini T, Heymann S, Bastian M (2014) ForceAtlas2, a continuous graph
812 layout algorithm for handy network visualization designed for the Gephi software.
813 J PloS one 9:e98679.
814 Johnson ZV, Walum H, Jamal YA, Xiao Y, Keebaugh AC, Inoue K, Young LJ (2015)
815 Central oxytocin receptors mediate mating-induced partner preferences and
816 enhance correlated activation across forebrain nuclei in male prairie voles. Horm
817 Behav 79:8-17.
818 Kabelik D, Weitekamp CA, Choudhury SC, Hartline JT, Smith AN, Hofmann HAJH,
819 behavior (2018) Neural activity in the social decision-making network of the
820 brown anole during reproductive and agonistic encounters. 106:178-188.
821 Keesom SM, Sloss BG, Erbowor-Becksen Z, Hurley LM (2017a) Social experience
822 alters socially induced serotonergic fluctuations in the inferior colliculus. Journal
823 of neurophysiology.
824 Keesom SM, Finton CJ, Sell GL, Hurley LM (2017b) Early-Life Social Isolation
825 Influences Mouse Ultrasonic Vocalizations during Male-Male Social Encounters.
826 PloS one 12:e0169705.
827 Keesom SM, Morningstar MD, Sandlain R, Wise BM, Hurley LM (2018) Social isolation
828 reduces serotonergic fiber density in the inferior colliculus of female, but not
829 male, mice. Brain research 1694:94-103.
830 Kim J, Lee S, Fang Y-Y, Shin A, Park S, Hashikawa K, Bhat S, Kim D, Sohn J-W, Lin D
831 (2019) Rapid, biphasic CRF neuronal responses encode positive and negative
832 valence. Nature neuroscience 22:576-585.
833 Koe BK, Weissman AJJoP, Therapeutics E (1966) p-Chlorophenylalanine: a specific
834 depletor of brain serotonin. 154:499-516.
835 Kohl J, Babayan BM, Rubinstein ND, Autry AE, Marin-Rodriguez B, Kapoor V,
836 Miyamishi K, Zweifel LS, Luo L, Uchida N, Catherine Dulac (2018) Functional
837 circuit architecture underlying parental behaviour. Nature 556:326.
838 Kovacs KJ (2008) Measurement of immediate-early gene activation- c-fos and beyond.
839 Journal of neuroendocrinology 20:665-672.

840 Lee H, Kim DW, Remedios R, Anthony TE, Chang A, Madisen L, Zeng H, Anderson DJ
841 (2014) Scalable control of mounting and attack by Esr1+ neurons in the
842 ventromedial hypothalamus. Nature 509:627-632.
843 Li B-H, Rowland NE (1993) Dexfenfluramine induces Fos-like immunoreactivity in
844 discrete brain regions in rats. Brain research bulletin 31:43-48.
845 Lin D, Boyle MP, Dollar P, Lee H, Lein E, Perona P, Anderson DJ (2011) Functional
846 identification of an aggression locus in the mouse hypothalamus. Nature
847 470:221.
848 Lupanova, A. S., & Egorova, M. A. (2015). Vocalization of sex partners in the house
849 mouse (Mus musculus). Journal of Evolutionary Biochemistry and Physiology,
850 51(4), 324-331.
851 Lynall M-E, Bassett DS, Kerwin R, McKenna PJ, Kitzbichler M, Muller U, Bullmore E
852 (2010) Functional connectivity and brain networks in schizophrenia. Journal of
853 Neuroscience 30:9477-9487.
854 Maney DL, Cho E, Goode CT (2006) Estrogen-dependent selectivity of genomic
855 responses to birdsong. The European journal of neuroscience 23:1523-1529.
856 Maney DL, Goode CT, Lange HS, Sanford SE, Solomon BL (2008) Estradiol modulates
857 neural responses to song in a seasonal songbird. The Journal of comparative
858 neurology 511:173-186.
859 Manouze H, Ghestem A, Poillerat V, Bennis M, Ba-M'hamed S, Benoliel J-J, Becker C,
860 Bernard C (2019) Effects of single cage housing on stress, cognitive, and seizure
861 parameters in the rat and mouse pilocarpine models of epilepsy. Eneuro 6.
862 Marlin BJ, Mitre M, D'amour JA, Chao MV, Froemke RC (2015) Oxytocin enables
863 maternal behaviour by balancing cortical inhibition. Nature.
864 Matthews, G. A., Nieh, E. H., Vander Weele, C. M., Halbert, S. A., Pradhan, R. V.,
865 Yosafat, A. S., ... & Tye, K. M. (2016). Dorsal raphe dopamine neurons represent
866 the experience of social isolation. Cell, 164(4), 617-631.
867 Matthews GA, Tye KM (2019) Neural mechanisms of social homeostasis. Annals of the
868 New York Academy of Sciences.
869 McEwen BS (2003) Early life influences on life-long patterns of behavior and health.
870 Mental retardation and developmental disabilities research reviews 9:149-154.
871 McHenry JA, Otis JM, Rossi MA, Robinson JE, Kosyk O, Miller NW, McElligott ZA,
872 Budygin EA, Rubinow DR, Stuber GD (2017) Hormonal gain control of a medial
873 preoptic area social reward circuit. Nature neuroscience 20:449.
874 Mumtaz F, Khan MI, Zubair M, Dehpour AR (2018) Neurobiology and consequences of
875 social isolation stress in animal model—A comprehensive review. Biomedicine &
876 Pharmacotherapy 105:1205-1222.
877 Muzerelle A, Scotto-Lomassese S, Bernard JF, Soiza-Reilly M, Gaspar P (2016)
878 Conditional anterograde tracing reveals distinct targeting of individual serotonin
879 cell groups (B5–B9) to the forebrain and brainstem. Brain Structure and Function
880 221:535-561.
881 Newman ME, Girvan M (2004) Finding and evaluating community structure in networks.
882 Physical review E 69:026113.
883 Newman SW (1999) The medial extended amygdala in male reproductive behavior. A
884 node in the mammalian social behavior network. Annals of the New York
885 Academy of Sciences 877:242-257.

886 Niederkofler V, Asher TE, Okaty BW, Rood BD, Narayan A, Hwa LS, Beck SG, Miczek
887 KA, Dymecki SM (2016) Identification of Serotonergic Neuronal Modules that
888 Affect Aggressive Behavior. Cell reports 17:1934-1949.
889 Niemczura, A. C., Grimsley, J. M., Kim, C., Alkhawaga, A., Poth, A., Carvalho, A., &
890 Wenstrup, J. J. (2020). Physiological and Behavioral Responses to Vocalization
891 Playback in Mice. Frontiers in Behavioral Neuroscience, 14.
892 O'Connell LA, Hofmann HA (2012) Evolution of a vertebrate social decision-making
893 network. Science 336:1154-1157.
894 Otchy TM, Wolff SB, Rhee JY, Pehlevan C, Kawai R, Kempf A, Gobes SM, Olveczky
895 BP (2015) Acute off-target effects of neural circuit manipulations. Nature
896 528:358-363.
897 Ouda L, Jilek M, Syka J (2016) Expression of c-Fos in rat auditory and limbic systems
898 following 22-kHz calls. Behavioural brain research 308:196-204.
899 Paxinos G, Franklin KB (2004) The mouse brain in stereotaxic coordinates: Gulf
900 Professional Publishing.
901 Pérez-González D, Malmierca MS, Covey E (2005) Novelty detector neurons in the
902 mammalian auditory midbrain. European Journal of Neuroscience 22:2879-2885.
903 Petersen CL, Hurley LM (2017) Putting it in Context: Linking Auditory Processing with
904 Social Behavior Circuits in the Vertebrate Brain. Integrative and comparative
905 biology.
906 Petersen CL, Timothy M, Kim DS, Bhandiwad AA, Mohr RA, Sisneros JA, Forlano PM
907 (2013) Exposure to advertisement calls of reproductive competitors activates
908 vocal-acoustic and catecholaminergic neurons in the plainfin midshipman fish,
909 Porichthys notatus. PloS one 8:e70474.
910 Portfors CV, Perkel DJ (2014) The role of ultrasonic vocalizations in mouse
911 communication. Current opinion in neurobiology 28:115-120.
912 Ren J, Friedmann D, Xiong J, Liu CD, Ferguson BR, Weerakkody T, DeLoach KE, Ran
913 C, Pun A, Sun Y (2018) Anatomically defined and functionally distinct dorsal
914 raphe serotonin sub-systems. Cell 175:472-487. e420.
915 Rogers-Carter MM, Christianson JP (2019) An insular view of the social decision-
916 making network. Neuroscience & Biobehavioral Reviews.
917 Ronald KL, Zhang X, Morrison MV, Miller R, Hurley LM (2020) Male mice adjust
918 courtship behavior in response to female multimodal signals. PloS one
919 15:e0229302.
920 Rothman RB, Baumann MH (2002) Serotonin releasing agents: neurochemical,
921 therapeutic and adverse effects. Pharmacology Biochemistry Behavior 71:825-
922 836.
923 Sangiamo DT, Warren MR, Neunuebel JP (2020) Ultrasonic signals associated with
924 different types of social behavior of mice. Nature neuroscience 23:411-422.
925 Schiller L, Jähkel M, Kretzschmar M, Brust P, Oehler J (2003) Autoradiographic
926 analyses of 5-HT1A and 5-HT2A receptors after social isolation in mice. Brain
927 research 980:169-178.
928 Schindelin J, Arganda-Carreras I, Frise E, Kaynig V, Longair M, Pietzsch T, Preibisch S,
929 Rueden C, Saalfeld S, Schmid B (2012) Fiji: an open-source platform for
930 biological-image analysis. Nature methods 9:676.

Schwarz LA, Miyamichi K, Gao XJ, Beier KT, Weissbourd B, DeLoach KE, Ren J, Ibanes S, Malenka RC, Kremer EJ (2015) Viral-genetic tracing of the input-output organization of a central noradrenaline circuit. Nature 524:88-92.

Seagraves KM, Arthur BJ, Egnor SR (2016) Evidence for an audience effect in mice: male social partners alter the male vocal response to female cues. Journal of Experimental Biology 219:1437-1448.

Singewald G, Nguyen N, Neumann I, Singewald N, Reber S (2009) Effect of chronic psychosocial stress-induced by subordinate colony (CSC) housing on brain neuronal activity patterns in mice. Stress 12:58-69.

Sporns O (2010) Networks of the Brain: MIT press.

Tanimizu T, Kenney JW, Okano E, Kadoma K, Frankland PW, Kida S (2017) Functional connectivity of multiple brain regions required for the consolidation of social recognition memory. Journal of Neuroscience 37:4103-4116.

Toth M, Tulogdi A, Biro L, Soros P, Mikics E, Haller J (2012) The neural background of hyper-emotional aggression induced by post-weaning social isolation. Behavioural brain research 233:120-129.

Tran, L., Lasher, B. K., Young, K. A., & Keele, N. B. (2013). Depletion of serotonin in the basolateral amygdala elevates glutamate receptors and facilitates fear-potentiated startle. Translational psychiatry, 3(9), e298-e298.

Tschida K, Michael V, Takatoh J, Han B-X, Zhao S, Sakurai K, Mooney R, Wang F (2019) A specialized neural circuit gates social vocalizations in the mouse. Neuron 103:459-472. e454.

VanElzakker, M., Fevurly, R. D., Breindel, T., & Spencer, R. L. (2008) Environmental novelty is
associated with a selective increase in Fos expression in the output elements of the hippocampal formation and the perirhinal cortex. Learning & Memory, 15(12), 899-908.

van den Heuvel MP, Sporns O (2019) A cross-disorder connectome landscape of brain dysconnectivity. Nature reviews neuroscience 20:435-446.

Van den Heuvel MP, Bullmore ET, Sporns O (2016) Comparative connectomics. Trends in cognitive sciences 20:345-361.

Warren M, Clein R, Spurrier M, Roth E, Neunuebel J (2020) Ultrashort-range, high-frequency communication by female mice shapes social interactions. Scientific reports 10:1-14.

Warren MR, Spurrier MS, Roth ED, Neunuebel JP (2018) Sex differences in vocal communication of freely interacting adult mice depend upon behavioral context. PloS one 13:e0204527.

Watts DJ, Strogatz SH (1998) Collective dynamics of ‘small-world’networks. Nature 393:440.

Wei Y-C, Wang S-R, Jiao Z-L, Zhang W, Lin J-K, Li X-Y, Li S-S, Zhang X, Xu X-H (2018) Medial preoptic area in mice is capable of mediating sexually dimorphic behaviors regardless of gender. Nature communications 9:279.

Weitekamp CA, Hofmann HA (2017) Neuromolecular correlates of cooperation and conflict during territory defense in a cichlid fish. Hormones and behavior 89:145-156.

977 Williamson CM, Klein IS, Lee W, Curley JP (2019) Immediate early gene activation
978 throughout the brain is associated with dynamic changes in social context. Social
979 neuroscience 14:253-265.
980 Wise T, Marwood L, Perkins A, Herane-Vives A, Joules R, Lythgoe D, Luh W, Williams
981 S, Young A, Cleare A (2017) Instability of default mode network connectivity in
982 major depression: a two-sample confirmation study. Translational psychiatry
983 7:e1105-e1105.
984
985

Figure legends:

Figure 1: Experimental design: playback paradigm and neuroanatomy. **A.** Male CBA/J mice arrived from Jackson Laboratories (Bar Harbor, ME) at 18 – 24 days postnatal, and were immediately separated into social (3 per cage) or isolated (1 per cage) housing **(B)**. **C.** mice remained in their respective housing conditions for 28 – 30 days. **D.** Saline (SAL) and fenfluramine (FEN) mice received saline injections for 3 days prior to playback; mice in the pCPA group received pCPA injections on these days. **E.** Forty-five minutes prior to playback trials, mice in the SAL and pCPA group received saline injections whereas FEN mice received fenfluramine. **F.** Playback trials were 60 minutes and consisted of 14 – 15 bursts of 5 female broadband vocalizations (BBVs). **G – L:** Representative inverse fluorescent 10X photomicrographs showing 7 nodes of the SBN: **G.** *Lateral septum* (LS); **H.** *Bed nucleus of the stria terminalis* (BNST); **I.** *Medial preoptic area* (mPOA); **J.** *Paraventricular nucleus* (PVN) and *anterior nucleus* (AH) of the hypothalamus; **K.** *ventromedial nucleus of the hypothalamus* (VMH); **L.** *Periaqueductal grey* (PAG). Additional abbreviations: anterior commissure (ac); lateral ventricle (lv); third ventricle (3v). Scale bar = 1mm (G), 500μm (H – L).

Figure 2: Summary linear mixed model analysis of cFos-ir within nodes of the SBN. **A – G**. All data are represented as arithmetic mean ± SEM between socially housed mice (green), and socially isolated mice (magenta). Asterisks represent main effects of drug treatment, ** $p < 0.001$, *** $p < 0.0001$. Letters indicate post-hoc differences (independent t test, p values corrected for multiple comparisons) in the case of housing by drug

1009 interaction. **H – I**. Representative photomicrographs in mPOA (H) and PVN (I) showing
1010 the effects of fenfluramine on cFos-ir in socially reared (H1/I1) or socially isolated (H2/I2)
1011 mice. Neurotrace (NT; blue), cFos-ir (magenta), scale bar = 250μm. Please see extended
1012 data figure 2-1 for a complete summary of *post hoc* analyses for linear mixed models
1013 performed within each SBN region.
1014
1015 **Figure 3.** Correlated patterns of cFos-ir are dependent on social experience. **A – F.**
1016 Heatmap matrices represent pairwise correlations between cFos-ir neurons with SBN
1017 nodes (boxes); colors indicate Pearson correlation coefficients. White boxes are self-
1018 correlations (r = 1); data are mirrored above and below the diagonal. **G.** Comparison
1019 between the absolute value of Pearson correlation coefficients between groups. Data are
1020 represented as mean ± SEM; letters indicate post-hoc differences (independent t test, p
1021 values corrected for multiple comparisons). **H.** Results of principal components analysis
1022 on covariation matrix derived from A – F. **I.** Distribution of PC1 scores between groups;
1023 data are represented as mean ± SEM. Please see extended data figure 3-1 for a complete
1024 summary of pairwise correlation statistics.
1025
1026 **Figure 4:** Correlated patterns of activity form different functional networks between
1027 treatment groups. **A – F.** Individual nodes are represented as green (SOC) or magenta
1028 (ISO) circles. The spatial distribution of nodes is determined by their individual strengths
1029 of correlation (Jacomy et al. 2014). Lines (edges) connecting nodes are indicative of
1030 statistically significant Pearson r values ($p < 0.05$); non-significant edges ($p > 0.05$) are
1031 excluded from graphs. **G – I:** Network measures vary between SOC and ISO mice. **G.**

SOC mice (green) have denser functional networks than ISO mice (magenta). **H.** SOC mice have higher clustering coefficients than ISO mice, whose clustering coefficient is zero in each drug treatment group. **I.** SOC mice formed fewer thus more densely populated functional communities than ISO mice.

Table 1: Summary of mixed linear models. Statistically significant main effects and interactions indicated with asterisks: * $p < 0.05$, ** $p < 0.01$, *** $p < 0.001$.

Table 2: Summary of group means with housing (a) and drug (b) treatments. Values expressed as arithmetic means ± SEM. Statistically significant differences group means indicated with asterisks: * $p < 0.05$, ** $p < 0.01$, *** $p < 0.001$. P values corrected for multiple comparisons (Benjamini, et al 2006).

Extended Data Figure 3-1: Summary of pairwise correlation statistics describing the relationship between cFos-ir neurons within SBN nodes.

Extended Data Figure 2-1: Complete summary of *post hoc* analyses for linear mixed models performed within each SBN region.

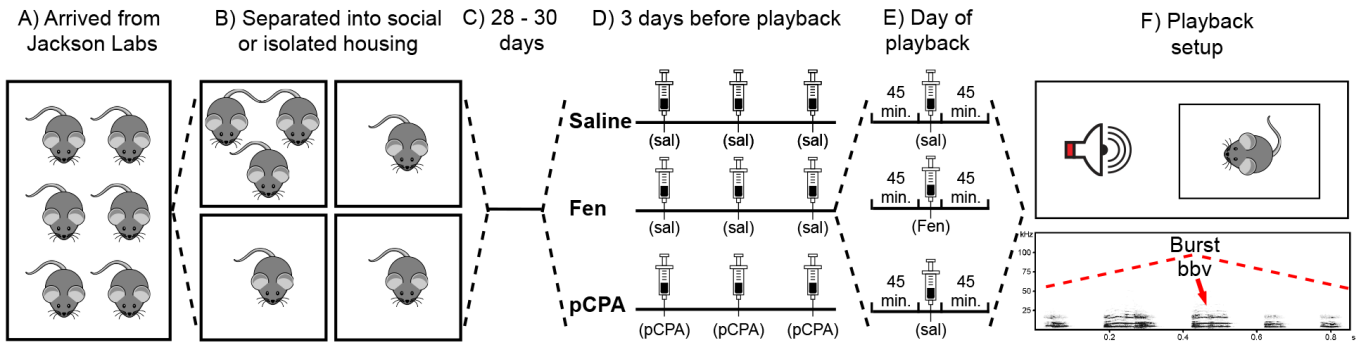

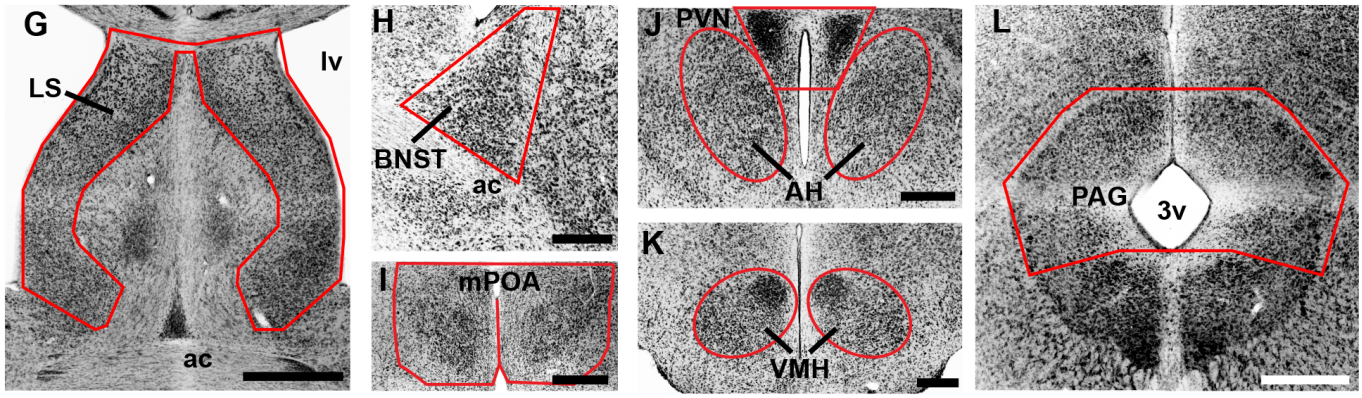

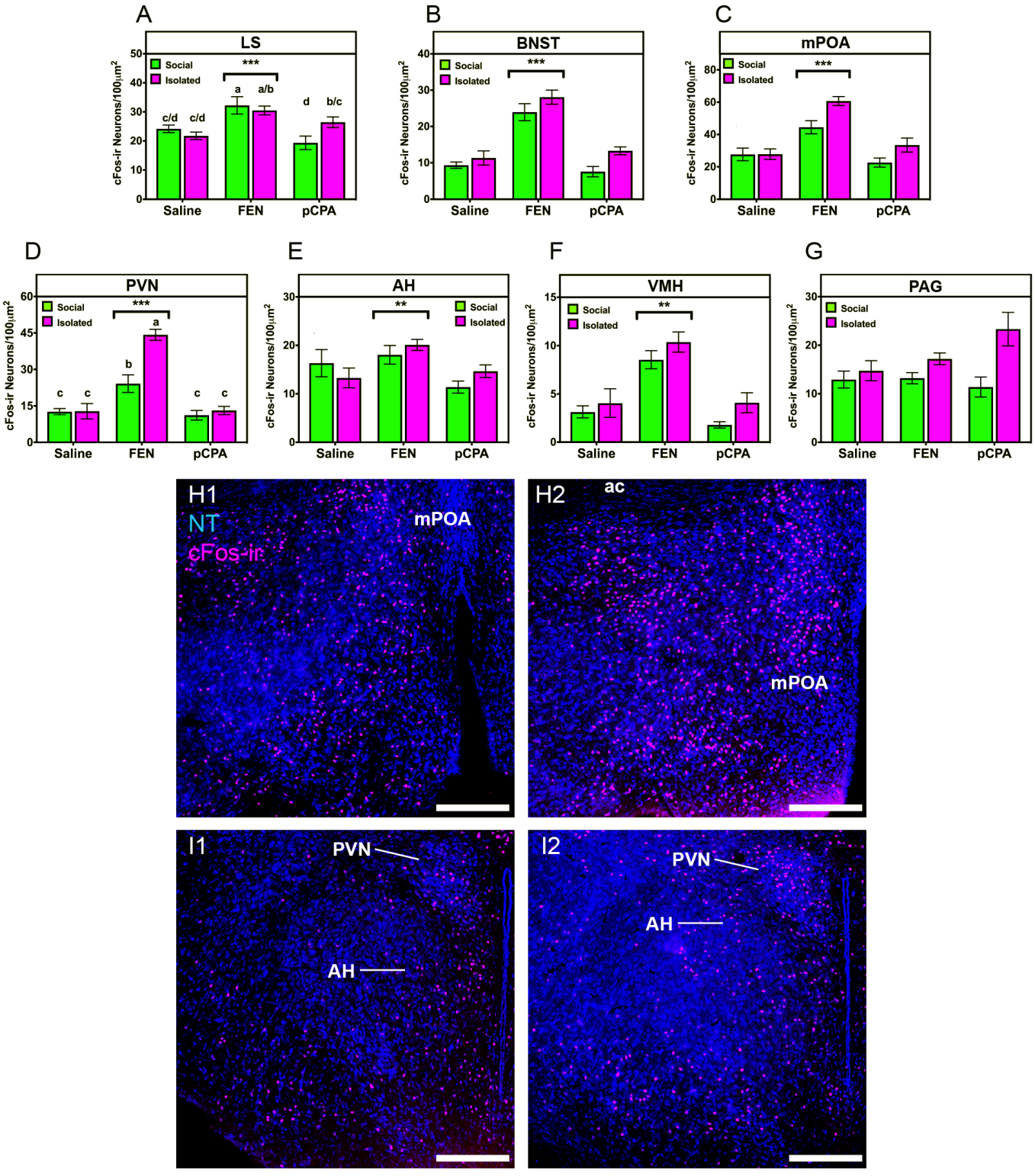

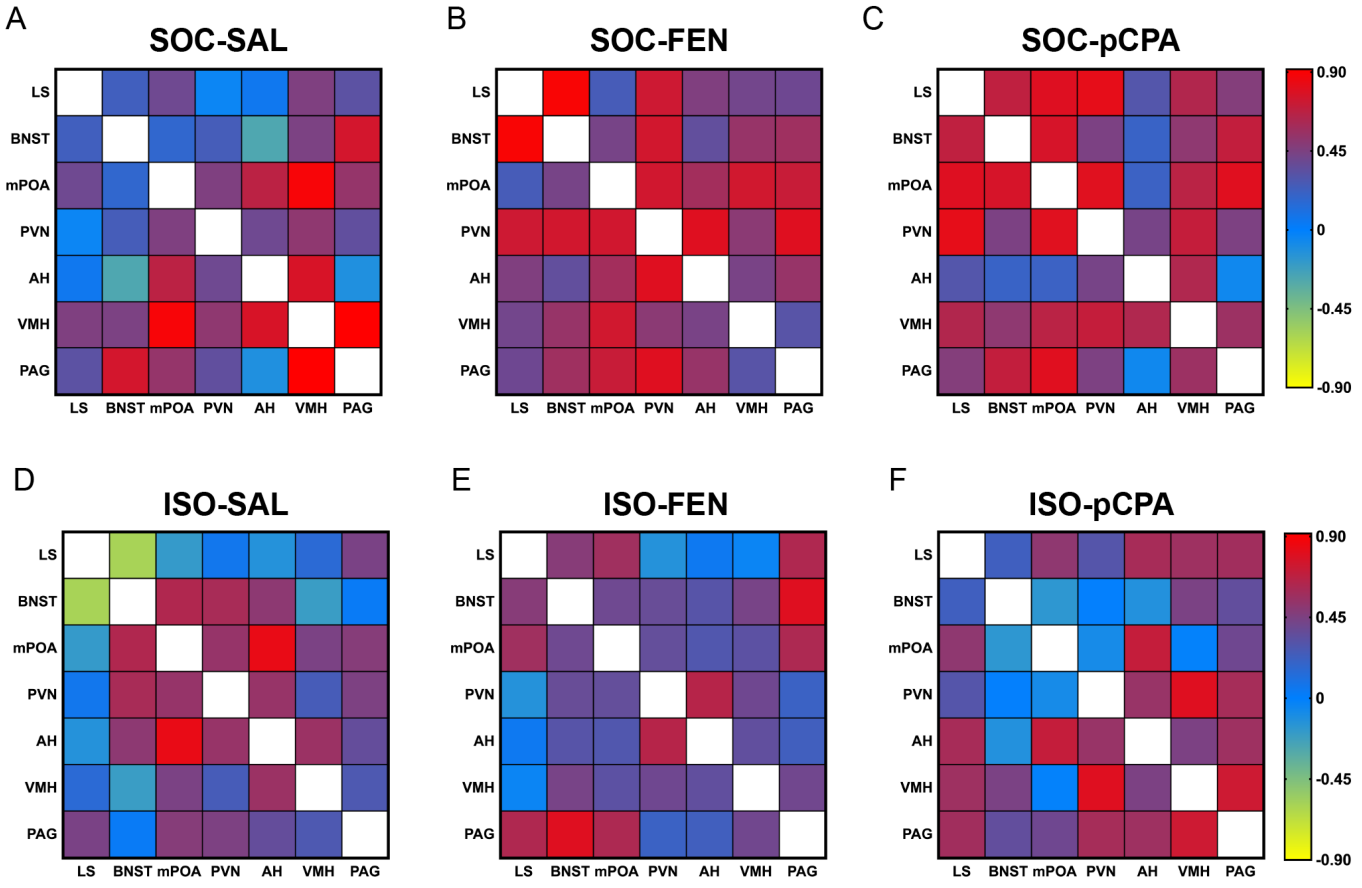

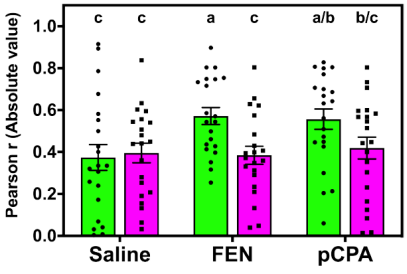

H

Eigenvalues			Eigenvectors		
PC	Eigenvalue	Percent	Region	PC1	PC2
1	**543.53**	**76.77**	LS	0.217	0.203
2	56.22	7.94	BNST	0.345	-0.165
3	39.69	5.61	**mPOA**	**0.682**	0.34
4	30.35	4.29	**PVN**	**0.553**	-0.548
5	20.82	2.94	AH	0.173	0.026
6	12.27	1.73	VMH	0.144	-0.019
7	5.09	0.72	PAG	0.115	0.716

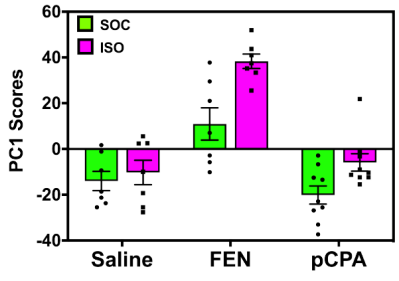

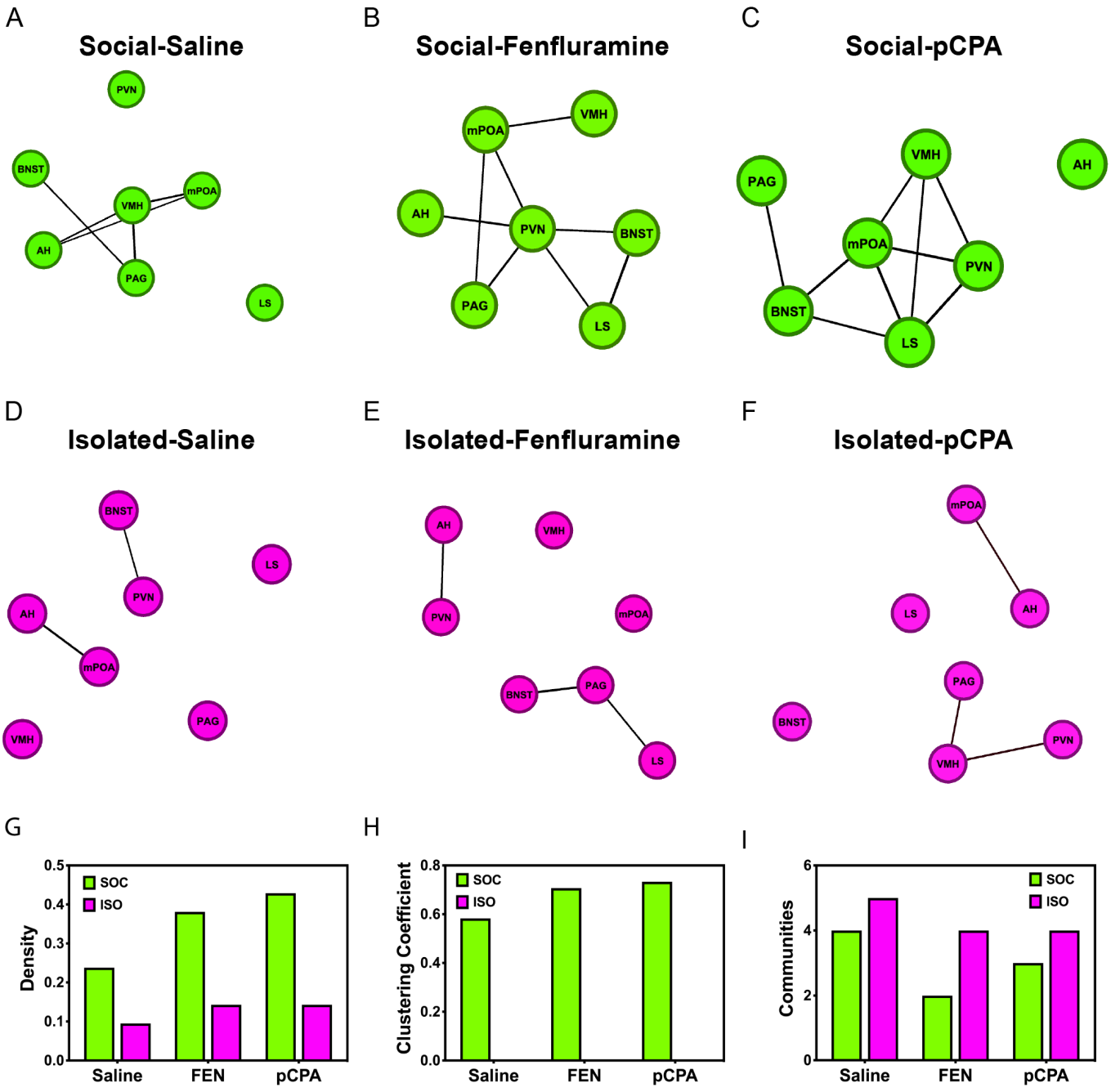

Table 1: Summary of linear mixed models assesing within-node effects of housing and drug treatment

Lateral Septum (LS)

Source	DF	F	P	Variance Component	Estimate	Std Error	95% Lower	95% Upper	P
Housing	1, 22.8	0.28	0.60	Cage number	-4.18	4.95	-13.89	5.53	0.40
Drug	2, 22.8	15.98	<.0001***	IHC Run	7.83	9.45	-10.70	26.36	0.41
Housing*Drug	2, 22.8	4.84	0.02*	Residual	33.51	8.33	21.73	58.40	

Bed Nucleus of the Stria Terminalis (BNST)

Source	DF	F	P	Variance Component	Estimate	Std Error	95% Lower	95% Upper	P
Housing	1, 14.5	7.23	0.02*	Cage number	3.15	6.84	-10.25	16.55	0.65
Drug	2, 14.5	52.63	<.0001***	IHC Run	2.80	4.31	-5.64	11.24	0.52
Housing*Drug	2, 14.5	0.49	0.62	Residual	20.98	6.70	12.23	44.13	

Meidal Preoptic Area (mPOA)

Source	DF	F	P	Variance Component	Estimate	Std Error	95% Lower	95% Upper	P
Housing	1, 20.5	6.67	0.02*	Cage number	57.24	24.33	9.56	104.93	0.02*
Drug	2, 20.5	25.34	<.0001***	IHC Run	34.86	40.78	-45.08	114.80	0.39
Housing*Drug	2, 20.5	1.96	0.17	Residual	28.66	10.54	15.59	69.15	

Paraventricular Nucleus of the Hypothalamus (PVN)

Source	DF	F	P	Variance Component	Estimate	Std Error	95% Lower	95% Upper	P
Housing	1, 19.1	10.12	0.005**	Cage number	21.13	12.54	-3.44	45.70	0.09
Drug	2, 19.1	40.99	<.0001***	IHC Run	13.95	17.01	-19.39	47.29	0.41
Housing*Drug	2, 19.1	8.25	0.003**	Residual	25.61	8.42	14.71	55.33	

Anterior Nucleus of the Hypothalamus (AH)

Source	DF	F	P	Variance Component	Estimate	Std Error	95% Lower	95% Upper	P
Housing	1, 21.2	0.18	0.67	Cage number	0.11	4.80	-9.29	9.51	0.98
Drug	2, 21.2	6.60	0.001**	IHC Run	4.92	6.33	-7.48	17.32	0.44
Housing*Drug	2, 21.2	1.91	0.17	Residual	24.55	6.49	15.53	44.58	

Ventromedial Nucleus of the Hypothalamus (VMH)

Source	DF	F	P	Variance Component	Estimate	Std Error	95% Lower	95% Upper	P
Housing	1, 21.5	2.52	0.13	Cage number	7.18	2.50	2.28	12.08	0.004**
Drug	2, 21.5	14.47	<.0001***	IHC Run	0.49	1.01	-1.48	2.46	0.63
Housing*Drug	2, 21.5	0.06	0.94	Residual	1.48	0.56	0.79	3.68	

Periaqueductal Gray (PAG)

Source	DF	F	P	Variance Component	Estimate	Std Error	95% Lower	95% Upper	P
Housing	1, 22.5	6.11	0.02*	Cage number	32.71	11.90	9.39	56.04	0.01**
Drug	2, 22.5	0.91	0.42	IHC Run	5.48	8.02	-10.24	21.21	0.49
Housing*Drug	2, 22.5	1.45	0.26	Residual	10.71	3.87	5.88	25.36	

Asterisks indicate statistical significance: * $p < 0.05$, ** $p < 0.01$, *** $p < 0.001$

Table 2a: Summary of arithmetic group means of cFos-ir neuron within housing treatments ± standard error

Housing	LS	BNST	mPOA	PVN	AH	VMH	PAG
Social	25.25 ± 3.8	13.6 ± 5.2	31.58 ± 6.6	15.97 ± 4.1	15.24 ± 2.0	4.48 ± 2.1	12.50 ± 0.6
Isolated	26.23 ± 2.5	17.56 ± 5.3*	40.65 ± 10.2*	23.39 ± 10.4**	16.00 ± 2.1	6.17 ± 2.1	18.42 ± 2.6*

Table 2b: Summary of arithmetic group means of cFos-ir neurons within drug treatments ± standard error

Drug treatment	LS	BNST	mPOA	PVN	AH	VMH	PAG
Saline	22.95 ± 1.2	10.32 ± 1.0	27.73 ± 0.1	12.71 ± 1.1	14.79 ± 1.5	3.587 ± 0.5	13.83 ± 0.9
Fenfluramine	31.36 ± 0.9**	26.0 ± 2.1***	52.59 ± 8.1***	34.2 ± 10.0***	19.06 ± 1.0*	9.458 ± 0.9***	15.2 ± 2.0
pCPA	22.9 ± 3.6	10.42 ± 2.9	28.02 ± 5.4	12.13 ± 1.0	13.02 ± 1.6	2.933 ± 1.2	17.35 ± 6.0

Values are exrpessed as mean ± SEM; statistically significant post hoc differences indicated by asterisks: * $p < 0.05$, ** $p < 0.01$, *** $p < 0.001$

Complete posthoc comparisons can be found in extended data Figure 2-1